Study of the Ion-Distribution Dynamics of an Aluminum Laser-Produced Plasma with Picosecond Resolution

M. Fajardo,[1,4] P. Audebert,[1] P. Renaudin,[2] H. Yashiro,[1,*] R. Shepherd,[3] J. C. Gauthier,[1] and C. Chenais-Popovics[1]

[1]*Laboratoire pour l'Utilisation des Lasers Intenses, UMR7605, CNRS-CEA-Université Paris VI-École Polytechnique, 91128 Palaiseau, France*

[2]*Commissariat à l'Énergie Atomique, 91680 Bruyères-le-Châtel, France*

[3]*Lawrence Livermore National Laboratory, P.O. Box 808, Livermore, California 94550*

[4]*GOLP, Instituto Superior Téchnico, 1 Avenida Rovisco Pais, Lisboa, Portugal*

(Received 18 September 2000)

The ion-distribution dynamics of an expanding aluminum plasma produced by a nanosecond laser pulse at moderate intensity (10^{13} W cm^{-2}) is studied by point-projection x-ray absorption spectroscopy with unprecedented, picosecond, time resolution. We show that the ionic populations measured as a function of distance to the target and at different probing times differ markedly from those predicted by widely accepted collisional radiative models coupled to hydrodynamic simulations. We discuss the effects of radiation, conduction, and expansion cooling on the spatiotemporal ionic distribution evolution.

DOI: 10.1103/PhysRevLett.86.1231 PACS numbers: 52.50.Jm, 52.25.Jm, 52.25.Os

Accurate calculations of multicharged ion population dynamics in plasmas not in local thermodynamic equilibrium (NLTE) are of paramount importance for understanding and diagnosing their radiative properties. Astrophysics and solar corona physics have played a key role in the development of these simulation capabilities [1]. As NLTE plasmas constitute a large majority of laboratory plasmas employed in x-ray laser research [2], laser-plasma x-ray sources [3], and x-ray driven fusion [4], the modeling of their ionization dynamics is also crucial for applications. A recent code workshop on the comparison of NLTE plasma kinetics demonstrated, as witnessed by the lack of agreement between the various case submissions, the depth of the problems to face [5]. Although simple models have been devised for ions in H-like, He-like, or Li-like ionization stages, such as the FLY code [6], there is an increased difficulty in describing partially filled L-shell configurations in low-Z materials in such conditions. Earlier experimental works have shown evidence of discrepancies between laboratory results and simulations [7–9] for recombining plasmas. These differences are not equally marked for all the experiments, but the general trend indicates that ionization at late times tends to be overestimated. A deficient knowledge of the atomic physics at stake could be the source of error. Effects of two-electron transitions [10], non-Maxwellian distributions [11], or the excited state dynamics during recombination [2] have been pointed out. On the other hand, some issues remain questionable in the hydrodynamic description of the plasma. Indeed, in the sub-10 eV, sub-solid-density ablating plasma region, there is a considerable difference between solid-state thermal conductivity models [12] and the Spitzer formalism usually used in plasma simulation, confirmed by experiments [13]. Two-dimensional effects could explain an expansion-increased lowering of the temperature and thus of ionization but the corresponding hydrodynamic simulations are difficult to access and their approximation by $1\frac{1}{2}$-D geometry remains tentative [14].

X-ray emission spectroscopy is a very powerful tool for the study of very hot plasmas, where the H-like and He-like transition lines and their dielectronic satellites can be recorded during and slightly after the laser pulse. In the recombination stage, however, colder, nonemitting Li-like to F-like ions can be seen only through absorption spectroscopy, which gives direct knowledge of these ionic species in the ground level. Because time resolution was relatively poor in previous experiments, the plasma could be probed only at late times (typically more than 1 ns after the laser maximum [7–9]), when the temporal temperature gradients are smoothed out. This makes it difficult to ascertain the cause for the low ionization obtained, for at such long time scales all the effects mentioned above had time to play a role. In this Letter, we give an account of the first experiment using the unique capability of chirped-pulse-amplification laser systems [15] of delivering synchronous subpicosecond and nanosecond laser pulses for x-ray backlighting and plasma production, respectively. We succeeded in obtaining a time and space ionization mapping of an expanding aluminum plasma from early to late times (0.2 to 1.4 ns) after the maximum of the laser pulse. The plasma was created by irradiating the side of an aluminum cylinder of 500 μm diameter with the 600 ps duration chirped beam of the 100 TW LULI laser facility. This pulse was frequency doubled ($\lambda = 0.53$ μm) and smoothed using a random phase plate. The energy on target was limited to 5–10 J (about 10^{13} W/cm^2 with a full width at half maximum focal spot diameter of 280 μm) in order to obtain a dominant He-like ionization state at peak irradiance. The main part of the beam was compressed into a 350 fs pulse, frequency doubled, and focused on a planar samarium (Sm) target with an off-axis parabola at an intensity of 10^{18} W/cm^2. The Sm plasma emitted a low

intensity (4×10^{12} photon/steradian/Å) quasicontinuum x-ray spectrum in the aluminum K_α spectral region (7.5 to 8.5 Å). The X-ray source dimension was measured to be 60 μm which was limiting the spatial resolution of the measurements. Its duration was measured to be below 10 ps. The $1s$-$2p$ absorption spectra were recorded for each shot using a flat ammonium dihydrogen phosphate (ADP) crystal spectrometer with a magnification of about 60, positioned at a 90° angle to the expansion axis, fitted to an x-ray sensitive charge-coupled device (CCD) camera.

Figure 1 shows an example of the absorption spectrum recorded at 800 ps delay. Each curve represents a 33.5 μm wide slice of the expanding plasma; its position relative to the initial surface is noted on the right-hand side. The absorption structures corresponding to Li-like to O-like aluminum ions present in the plasma are indicated. In all spectra, the He_α line, the intercombination line, and the Li-like satellite lines are clearly present in emission. In some spectra, the cold K_α line was also recorded. At 200 ps delay, plasma expansion is less than 35 μm. Absorption features from Al^{8+} to Al^{10+} are visible. At 500 ps delay, the lowest ionization stage Al^{7+} is located very close to the target (less than 50 μm) but the Li-like ions are present farther away, up to 150 μm distance to the target surface. Later in time at 1400 ps delay, the plasma is less ionized (F-like to C-like, i.e., Al^{4+} to Al^{7+}) and the ions are homogeneous throughout the entire plasma volume (up to 200 μm of the target, i.e., the totality of the observation field).

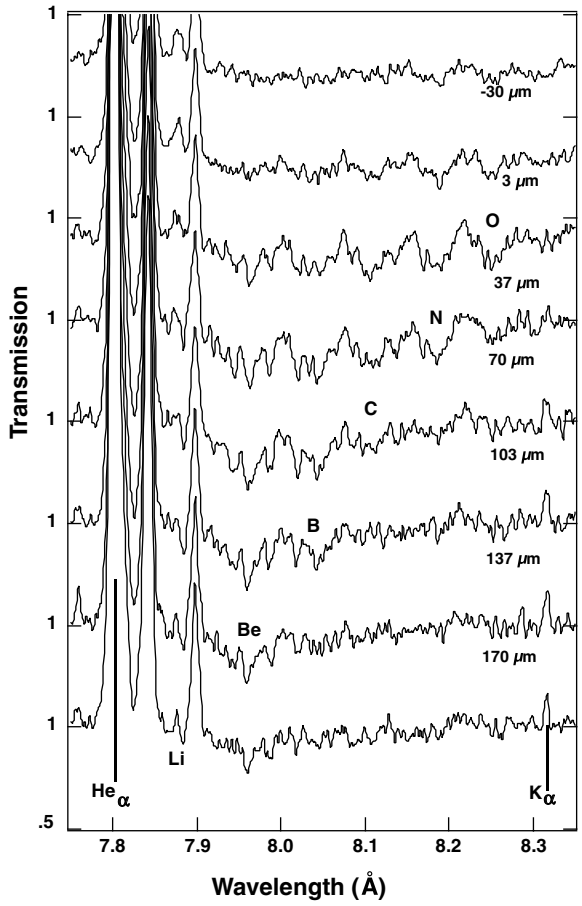

FIG. 1. Transmission of the picosecond duration Sm backlighter as a function of position in front of the target plane for a delay of 800 ps after the peak of the plasma producing laser pulse. Transmission curves for each position have been shifted by 0.5 for visibility.

Each absorption spectrum obtained for a specific time and position was analyzed using the HULLAC code [16]. The absorption spectrum as a function of plasma parameters (temperature, areal mass, ion populations) was calculated and convolved with the experimental spectral resolution of 2 eV. Relative populations for each ion could be approximated using LTE or inserted manually. Since the examined plasma is strongly NLTE, the second method was used. Indeed, upon verification, single-temperature LTE spectra could not fit experimental results, giving an ion distribution more peaked than what was observed. Systematic analysis of the measured spectra for each position and time was performed using a genetic algorithm, a robust approach for automated analysis of x-ray line spectra [17], from which the populations for the Al^{4+} to Al^{9+} ion species could be obtained. Li-like and He-like ionic fractions were impossible to determine, because their time-integrated emission was superimposed on the absorption. To cross-check our results, a multiconfiguration Dirac-Fock code (MCDF) [18] was also used to analyze the spectra independently, giving consistent results.

To provide a synthetic vision of the results, a partial ionization state Z_{par} can be calculated, defined by $Z_{\mathrm{par}} = \sum_i f_i Z_i / \sum_i f_i$, f_i being the ionic fraction of the ion Z_i, Z_i ranging from 4 to 9. The results are shown in Fig. 2 for the different probing times. The displacement of the ionization gradient as a function of time is clearly visible, as well as the low ionization level reached at late times. Delay time errors were less than 30 ps. At 800 and 1400 ps, the bulk of the ionic population lies among the quantifiable ions, so that the experimental error is dominated by the background of the CCD. For earlier times, however, the apparent absorbing ions correspond to the tail of the ionic distribution which peaks over Li-like. The experimental error increases inversely with the relative absorption signal making the region in the shadow of the target (around the origin in Fig. 2) less reliable. The experimental laser flux was not thoroughly characterized at full power, but it was estimated that 80% of the energy of the beam was within a 140 μm radius focal spot. Errors in measured laser energy were on the order of 20%. The fact that the target was cylindrical plays no role in the low charge of ions that was observed. From geometry considerations, plasmas that were eventually created at large angles relative to the laser axis should be hidden in absorption or observable only at much later times (after expansion).

The widely accepted assumption that the radiation transport plays little role for low-Z materials such as aluminum at low irradiances led us to try to compare our experimental

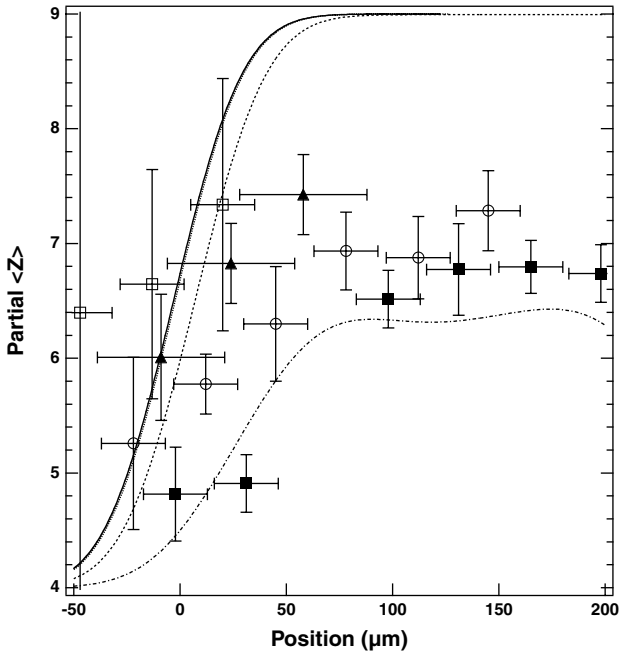

FIG. 2. Measured partial ionization Z_{par} as a function of the distance normal to the target at 200 ps (open squares), 500 ps (filled triangles), 800 ps (open circles), and 1400 ps (filled squares) after the peak of the laser pulse. Results from hydrocode and time-dependent collisional-radiative simulations are also given at 200 ps (solid line), 500 ps (dashed line, hidden by the 200 ps solid line), 800 ps (dotted line), and 1400 ps (dash-dotted line). Laser intensity is 5×10^{13} W/cm^2.

results with those simulated by FILM, a 1D Lagrangian hydrodynamics code that does not describe radiative transport but includes a detailed, non-LTE, atomic physics treatment suited for the ion range that was observed [19]. Two disagreements are apparent: in the coronal plasma, the resulting ionization is much higher than actually measured ($\langle Z \rangle \approx 11$ at 1400 ps), and, in the high-density, low-temperature region, steep ionization gradients are close to the target (within 0 to 10 μm, from 200 to 1400 ps). Although the gradient was smoothed experimentally due to the 60 μm size of the backlighter, its position relative to the surface of the target was well calibrated and could not be reproduced by the simulation. To improve the description of the coronal plasma, a version of the code that includes self-similar lateral expansion effects ($1\frac{1}{2}$-D) was used, and indeed the electronic temperature was lowered by 30%–40% at later times, at 200 μm from the target. The effect of dielectronic recombination was investigated by postprocessing the FILM data with the average-ion time-dependent model NIMP [20] but could account only for a 0.25 lowering of $\langle Z \rangle$ in the corona at late times (2000 ps) while increasing it by the same amount during the laser pulse because of the effect of excitation-autoionization processes.

The effect of radiation transport was first determined using MULTI [21], a 1D hydrocode that includes multigroup radiation transport using the diffusion approximation. We found a significant lowering of T_e in the dense reemission zone of the plasma. This effect becomes patently obvious at 1400 ps, when this colder region has expanded into the spectrograph line of sight, pushing the temperature gradient roughly 50 μm away from the surface of the target. Finally, the combination of radiation transport and lateral expansion effects was taken into account by CHIVAS, a hydrocode that uses time-dependent average-ion atomic physics [14] but neglects two-electron transitions. An interesting feature of CHIVAS is that it includes an optional self-similar lateral temperature conduction model with Spitzer nonlinear heat conduction in a constant density medium [22]. Evidence of the beneficial influence of lateral conduction cooling in the modeling of the Se x-ray laser had been demonstrated [14]. The resulting profiles of N_e and T_e at different times are shown in Fig. 3. The temperature is much lower than predicted by the other codes (roughly 25 eV at 200 μm at 1400 ps, compared to 60 eV with FILM $1\frac{1}{2}$-D, 110 eV with FILM 1D, and 95 eV with MULTI 1D). Because the atomic physics packages available in these various hydrocodes lack precision to compare with detailed experiments, we used the NLTE atomic physics code TRANSPEC as a postprocessor of CHIVAS, using the newest version which includes superconfigurations up to $n = 6$ to deal with multielectron transition processes [23]. The resulting average ionization, obtained for a 5×10^{13} W/cm^2 irradiance and convolved with the spatial resolution is shown in Fig. 2 and is in good agreement with the experimental data at 1400 ps. The ionic fractions calculated are also in good agreement with the experiment.

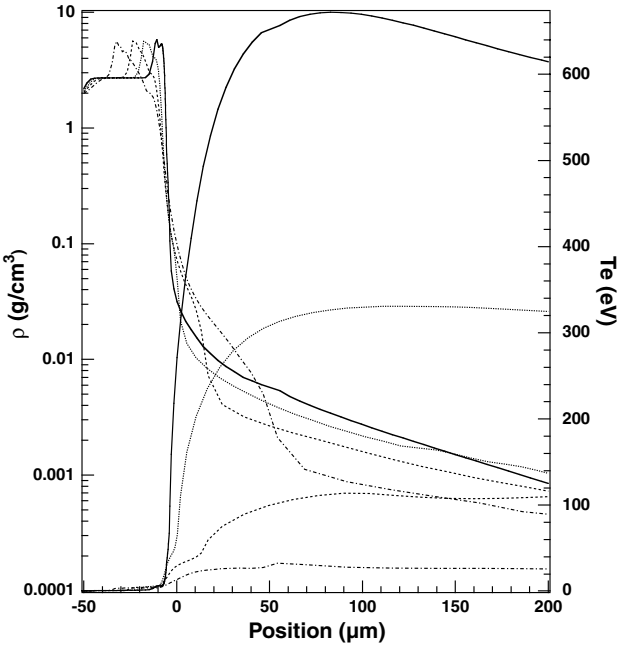

FIG. 3. CHIVAS predictions of matter density (left) and electron temperature (right) as a function of position in front of the target and time after the peak of the laser pulse, 200 ps (solid line), 500 ps (dashed line), 800 ps (dotted line), and 1400 ps (dash-dotted line). Laser intensity is 5×10^{13} W/cm^2.

Although we are able to explain the experimental spectra at 1400 ps, the predicted average ionization at earlier times is much higher and steeper than observed. At 800 ps, for instance, the plasma should be more than Li-like beyond 30 μm from the target surface according to simulations. The observed ionic distribution, on the contrary, peaks at about $\langle Z \rangle = 7$ (C-like) at 160 μm from the surface. At 200 and 500 ps no quantitative conclusions can be inferred, because the maximum of the absorption structure is hidden by the He_α and satellite emission. It seems probable that ionization lowering arises earlier than calculated, suggesting that the lateral expansion had a greater velocity than foreseen.

The reason for this phenomenon is most likely to be purely hydrodynamic, lying in either lateral heat transport, lateral expansion, incorrect description of the conductivity effects, or a combination of all of the above. For instance, Lee and More's conductivity model shows that thermal conductivity evaluated with the classical Spitzer formula is underestimated by a factor of 100 for low-temperature, high-density plasmas. The effect of the improved conductivity would be an increased heat flow into the near-solid-density regions behind the ablation front, intermediate density regions becoming less heated. Crude simulations were performed, multiplying by 100 the conductivity of the cells in the conversion region (behind the ablation front at the maximum of the pulse) showing a cold region propagating outwards and pushing the temperature gradient further up to 50 μm from the target at 800 ps as observed. The size of the focal spot is a determining factor for the time of appearance of lateral expansion effects. More simulations were run with smaller focal radii but keeping the laser intensity constant. They showed that the temperature drop that occurs at 1200 ps after the laser for the nominal 280 μm diameter focal spot (see Fig. 3) becomes apparent at 1000 ps for a 200 μm focal spot and as early as 700 ps for a 140 μm focal spot. These simulations show how sensitive the time scales can be to 2D effects.

We have obtained an ionization mapping of a freely expanding plasma from early times to its relaxation by absorption spectroscopy using picosecond x-ray backlighting. With the help of exhaustive modeling, some important conclusions have been reached. At late times (1400 ps), the low-density, cold region near the surface is the result of the expansion of the inner part of the target, the so-called reemission zone. An improved conductivity model should be used in this region to enhance the resulting detachment of the ionization gradient from the surface of the target. In the corona, 2D effects can dramatically cool down the plasma. However, atomic physics models must follow the rapid lowering of the temperature, and this is achieved only when using time-dependent NLTE detailed atomic physics modeling. The low values of $\langle Z \rangle$ are thus explained without resorting to dielectronic recombination, which induces no significant change in the ionization. At earlier times (800 ps), the measured ionization is much lower than predicted, suggesting that the 2D hydrodynamic effects arise earlier. In order to understand this phenomenon, it would be useful to use varied-size microdot targets in later experiments.

We gratefully acknowledge J. Bruneau, S. Jacquemot, O. Peyrusse, and A. Decoster for valuable discussions and their help in MCDF calculations and the use of the CHIVAS and TRANSPEC codes. We appreciate the help of S. Rose in providing unpublished results of Al ionization including two-electron transitions. One of us (M. F.) was financed through MCT (Portugal) under Contract No. PRAXIS XXI/BD/13732/97.

*Present address: Electrotechnical Laboratory, Tsukuba, Japan.

[1] J. Oxenius, *Kinetic Theory of Particles and Photons* (Springer-Verlag, Berlin, 1986).
[2] R. C. Elton, *X-Ray Lasers* (Academic Press, San Diego, 1990).
[3] I. C. Turcu and J. B. Dance, *X-Rays from Laser Plasmas* (Wiley, Chichester, 1999).
[4] J. Lindl, Phys. Plasmas **2**, 3933 (1995).
[5] R. W. Lee, J. K. Nash, and Y. Ralchenko, J. Quant. Spectrosc. Radiat. Transfer **58**, 737 (1997).
[6] R. W. Lee, B. L. Whitten, and R. E. Strout, J. Quant. Spectrosc. Radiat. Transfer **54**, 81 (1995); R. W. Lee and J. T. Larsen, J. Quant. Spectrosc. Radiat. Transfer **56**, 535 (1996)
[7] C. A. Back *et al.,* Phys. Rev. A **46**, 3405 (1992).
[8] S. Gary *et al.,* J. Quant. Spectrosc. Radiat. Transfer **54**, 155 (1995).
[9] A. Klisnick *et al.,* Phys. Rev. E **53**, 5315 (1996).
[10] J. R. Albritton and B. G. Wilson, Phys. Rev. Lett. **83**, 1594 (1999); J. Quant. Spectrosc. Radiat. Transfer **65**, 1 (2000).
[11] F. B. Rosmej, J. Phys. B **30**, L819 (1997).
[12] Y. T. Lee and R. M. More, Phys. Fluids **27**, 1273 (1984).
[13] C. Quoix *et al.,* J. Quant. Spectrosc. Radiat. Transfer **65**, 455 (2000).
[14] S. Jacquemot *et al.,* in *Proceedings of Ultra-Short Wavelength Lasers II,* SPIE Proceedings Vol. 2012 (SPIE–International Society for Optical Engineering, Bellingham, WA, 1994), p. 180.
[15] D. Strickland and G. Mourou, Opt. Commun. **56**, 219 (1985).
[16] M. Klapisch *et al.,* J. Opt. Soc. Am. B **61**, 148 (1977).
[17] I. Golovkin, R. Mancini, and S. Louis, in *Proceedings of the Genetic and Evolutionary Computational Conference, 1999, Orlando, FL* (Morgan Kaufmann, San Francisco, 1999), pp. 1529–1534.
[18] J. Bruneau, J. Phys. B **17**, 3009 (1989).
[19] M. Busquet, J.-P. Raucourt, and J.-C. Gauthier, J. Quant. Spectrosc. Radiat. Transfer **54**, 81 (1995).
[20] S. Rose, Rutherford Appleton Laboratory Technical Report No. RAL-TR-97-020, 1997.
[21] R. Ramis, R. F. Schmalz, and J. Meyer-ter-Vehn, Comput. Phys. Commun. **49**, 475 (1988).
[22] A. Decoster (private communication).
[23] O. Peyrusse, J. Phys. B **32**, 683 (1999).